



# CHORUS

This is the accepted manuscript made available via CHORUS. The article has been published as:

## Strong effect of electron-phonon interaction on the lattice thermal conductivity in 3C-SiC

Tianshi Wang, Zhigang Gui, Anderson Janotti, Chaoying Ni, and Prashant Karandikar  
Phys. Rev. Materials **1**, 034601 — Published 3 August 2017

DOI: [10.1103/PhysRevMaterials.1.034601](https://doi.org/10.1103/PhysRevMaterials.1.034601)

1 **The strong effect of electron-phonon interaction on the lattice**  
2 **thermal conductivity in 3C-SiC**

3 Tianshi Wang, Zhigang Gui, Anderson Janotti, and Chaoying Ni

4 *Department of Materials Science and Engineering,*

5 *University of Delaware, Newark, DE 19716.*

6 Prashant Karandikar

7 *M-Cubed Technologies, Inc., Newark, Delaware 19711, USA*

8 (Dated: July 14, 2017)

### Abstract

3C-SiC is a promising semiconductor for many applications where doping and heat dissipation are fundamental parameters in the device design. However, the variation of thermal conductivity with carrier concentration remains to be explored. Using density functional theory, we computed the lattice thermal conductivity in intrinsic and doped 3C-SiC with charge carrier concentrations in the range of  $10^{17}$  to  $10^{21}$   $\text{cm}^{-3}$ . From the calculated phonon dispersion, group velocities, and phonon-phonon scattering rates for undoped bulk 3C-SiC, we obtain a thermal conductivity of 491 W/mK at 300 K. In the case of doped 3C-SiC, we find that the lattice thermal conductivity is strongly reduced at high carrier concentrations. We also predict the effects of electron-phonon interaction (EPI) to be much stronger for hole- than electron-doped material, which is explained by the features of the electronic band structure near the band edges. In the limit of high carrier concentration of  $10^{21}$   $\text{cm}^{-3}$ , the thermal conductivity drops by 57% for hole and 32% for electron doping. Our results and analysis provide an in-depth understanding of phonon transport for the design of novel SiC-based electronics.

## 9 I. INTRODUCTION

10 SiC combines a series of desired properties for high-power electronic applications, such as  
11 wide band gap,<sup>1</sup> high thermal conductivity and high breakdown voltage.<sup>2</sup> Among the many  
12 existing polytypes, 3C-SiC has the simple isotropic zinc blende crystal structure. 3C-SiC has  
13 several advantages comparing to other polytypes. It can grow heteroepitaxially on silicon  
14 substrates<sup>3</sup> and is a promising material for mechanical and thermal sensors.<sup>4</sup> 3C-SiC is also  
15 used to fabricate light-emitting diodes<sup>5</sup> and serves as substrate in the growth of graphene.<sup>6</sup>  
16 The lattice thermal conductivity of 3C-SiC is an important parameter not only for high  
17 power devices, but also for substrate temperature control and uniformity during epitaxial  
18 growth and for device packaging design.

19 Experimental data for thermal conductivity in intrinsic or doped 3C-SiC are scarce, in  
20 part due to the difficulty of growing crystals with high structural quality.<sup>7</sup> Morelli *et al.*<sup>8</sup>  
21 obtained a value of 330 W/mK at room temperature for a polycrystalline sample, and  
22 suggested that their result is limited by scattering from grain boundaries. This value is  
23 much lower than those reported for the structurally more complex hexagonal 4H- or 6H-SiC  
24 polytypes.<sup>9,10</sup> Since in many applications of interest the 3C-SiC is doped with high carrier  
25 densities, of  $10^{19}$  cm<sup>-3</sup> or even  $10^{21}$  cm<sup>-3</sup>,<sup>4,11</sup> it is essential to understand the role of the  
26 electron-phonon interaction on the thermal conductivity of electron- and hole-doped SiC.  
27 Both theory<sup>12</sup> and experiments<sup>13</sup> reveal that the impact of electron-phonon interaction on  
28 the thermal conductivity in silicon is significant at room temperature. Such effect has not  
29 yet been investigated for SiC.

30 Here we use first-principles calculations to predict the heat transport properties in in-  
31 trinsic and doped SiC. Due to the limitation in computational resources, this study focuses  
32 on 3C-SiC. Calculations for 4H- and 6H-SiC would require much more computational effort  
33 due to larger number of atoms in the primitive cell. However, we believe our results also  
34 apply these other SiC polymorphs, due to the similarities in crystal structure, especially in  
35 the in-plane directions of the hexagonal 2H, 4H, and 6H polytypes. The approach offers the  
36 advantage of being free of any adjustable parameters and has a general applicability. In the  
37 following, we describe the details of the calculations, present the results for the phonon dis-  
38 persion, the phonon-phonon scattering and the lattice thermal conductivity in intrinsic SiC.  
39 We then present the calculated electron-phonon scattering rates, and predict the impact of

40 the carrier concentration on thermal conductivity for electron- and hole-doped 3C-SiC. The  
 41 effect of phonon scattering with natural Si and C isotopes is included in all the calculations.

## 42 II. COMPUTATIONAL APPROACH

43 The intrinsic thermal conductivity tensor can be solved iteratively using Boltzmann trans-  
 44 port equation (BTE):<sup>14</sup>

$$\kappa^{\alpha\beta} = \frac{1}{k_B T^2 \Omega N} \sum_{\lambda} n_{\lambda}^0 (n_{\lambda}^0 + 1) (\hbar \omega_{\lambda})^2 v_{\lambda}^{\alpha} v_{\lambda}^{\beta} \tau_{\lambda}, \quad (1)$$

45 where  $\alpha$  and  $\beta$  are the cartesian components,  $\Omega$  is the volume of the primitive cell, and  $N$   
 46 denotes the number of  $\mathbf{q}$  points in a grid used to sample the Brillouin zone;  $\lambda$  denotes a  
 47 phonon mode with polarization  $\nu$  and wave vector  $\mathbf{q}$ ,  $\omega_{\lambda}$  is the angular frequency for the  
 48 phonon mode  $\lambda$ , and  $n_{\lambda}^0$  is the Bose-Einstein distribution function;  $v_{\lambda}^{\alpha}$  is the projection of the  
 49 phonon group velocity along the direction  $\alpha$ . Finally,  $\tau_{\lambda}$  denotes the phonon lifetime, which  
 50 is the inverse of the scattering rate  $\Gamma_{\lambda}$ . The scattering rate contains the contributions from  
 51 the phonon-phonon scattering, isotopic effect, EPI, etc., as described by the Matthiessen's  
 52 rule.

53 The phonon-phonon scattering which is the dominant factor in intrinsic thermal con-  
 54 ductivity is calculated based on the density functional theory (DFT)<sup>15,16</sup> and the density  
 55 functional perturbation theory (DFPT).<sup>17,18</sup> We first calculate the second order interatomic  
 56 force constants (IFCs) from DFPT and obtain the phonon frequency and group velocity for  
 57 each phonon in a grid. The third order IFCs are derived using the finite difference method  
 58 from a set of force-displacement data obtained from DFT calculations. With the third order  
 59 IFC, we obtain the scattering matrix elements  $V_{\lambda\lambda'\lambda''}$  as described in Ref. 14. We then solve  
 60 the three-phonon scattering rates  $\Gamma_{\lambda\lambda'\lambda''}^{\pm}$  from the Fermi's golden rule as:<sup>14,19</sup>

$$\Gamma_{\lambda\lambda'\lambda''}^{\pm} = \frac{\hbar\pi}{4} \left\{ \begin{array}{l} n' - n'' \\ n' + n'' + 1 \end{array} \right\} \frac{\delta(\omega \pm \omega' - \omega'')}{\omega\omega'\omega''} |V_{\lambda\lambda'\lambda''}^{\pm}|^2, \quad (2)$$

61 where the upper (lower) row in the curly brackets follows the + (−) sign, which corresponds  
 62 to the absorption (emission) processes.  $n'$  stands for  $n_{\lambda'}^0$ , and so forth. The effect of isotopic  
 63 disorder on the phonon scattering rate in intrinsic SiC is included using the Matthiessen's  
 64 rule as described in Ref. 19 taking the Si and C natural isotopic distributions from Ref. 20.

65 The thermal conductivity of the doped material is calculated by incorporating the phonon  
 66 scattering rate due to the EPI, which is related to the imaginary part of the phonon self-  
 67 energy, and is calculated using Fermi's golden rule as:<sup>21,22</sup>

$$\frac{1}{\tau_{\mathbf{q}\nu}^{\text{ph}}} = \frac{2\pi}{\hbar} 2 \sum_{mn} \int \frac{d\mathbf{k}}{\Omega_{\text{BZ}}} |g_{mn\nu}(\mathbf{k}, \mathbf{q})|^2 (f_{n\mathbf{k}} - f_{m\mathbf{k}+\mathbf{q}}) \times \delta(\varepsilon_{m\mathbf{k}+\mathbf{q}} - \varepsilon_{n\mathbf{k}} - \hbar\omega_{\mathbf{q}\nu}), \quad (3)$$

68 where  $\Omega_{\text{BZ}}$  is the volume of the Brillouin zone, and  $f_{n\mathbf{k}}$  is the distribution function for elec-  
 69 trons. The factor of 2 before the summation accounts for the spin degeneracy. The matrix  
 70 element  $g_{mn\nu}(\mathbf{k}, \mathbf{q})$  of one electron-phonon scattering process involves a phonon with polar-  
 71 ization  $\nu$  and two electrons with band indices  $m$  and  $n$ . It can be derived from DFPT using  
 72  $g_{mn\nu}(\mathbf{k}, \mathbf{q}) = \frac{1}{\sqrt{2\omega_{\mathbf{q}\nu}}} \langle \psi_{m\mathbf{k}+\mathbf{q}} | \partial_{\mathbf{q}\nu} V | \psi_{n\mathbf{k}} \rangle$ .<sup>23</sup> Note that the phase changes after scattering should  
 73 not change the value of  $|g_{mn\nu}(\mathbf{k}, \mathbf{q})|^2$  and the derived scattering rates. The calculations are  
 74 quite computationally consuming because a proper description of the scattering processes  
 75 requires convergence using very fine meshes in the Brillouin zone. To lower the computa-  
 76 tional cost, we employ the recently developed interpolation techniques based on maximally  
 77 localized Wannier function (MLWF) transformation<sup>22,24,25</sup> which have successfully provided  
 78 accurate results for other materials.<sup>23,25</sup> We then derive the phonon scattering rates for each  
 79 mode using the Matthiessen's rule by combining the results from the electron-phonon inter-  
 80 action and the results from iteratively solving for the intrinsic material. Finally, we obtain  
 81 the thermal conductivity of doped materials using Eq. (1).

82 We use the Quantum ESPRESSO package<sup>26</sup> for the DFT and DFPT calculations, within  
 83 the local density approximation (LDA).<sup>27</sup> Norm-conserving pseudopotentials<sup>28</sup> and a plane  
 84 wave cut-off of 100 Ry are employed. We first perform structural optimization using a  
 85  $12 \times 12 \times 12$   $\mathbf{k}$ -point mesh ( $\mathbf{k}$ -mesh). The convergence tolerance of total energy is set  
 86 to  $10^{-12}$  Ry. The calculated equilibrium lattice parameter is 4.342 Å, in good agreement  
 87 with the experimental value of 4.360 Å.<sup>29</sup> In the phonon calculations, the dynamic matrices  
 88 and second order IFCs are computed on a  $6 \times 6 \times 6$   $\mathbf{q}$ -point mesh ( $\mathbf{q}$ -mesh). In the third  
 89 order IFCs calculations, a cutoff of 5.025 Å (or up to the fifth nearest-neighbor atoms) is  
 90 chosen for the interaction range after comparing with the results using 4.537 Å (i.e., up  
 91 to the fourth nearest-neighbor atoms). We generate 204 displaced supercells, each with  
 92 250 atoms, with the atomic displacements of 0.021 Å. The ShengBTE package<sup>19</sup> is used for  
 93 obtaining the third order IFCs and for solving the phonon Boltzmann transport equation  
 94 (BTE) iteratively. When solving the BTE, we performed convergence tests with respect to

95 the  $\mathbf{q}$ -mesh. Tests using  $\mathbf{q}$ -meshes of  $40 \times 40 \times 40$  and  $35 \times 35 \times 35$  give less than 0.5%  
96 differences. For convenience, we choose the latter as  $\mathbf{q}$ -mesh size. We also repeated the  
97 calculations using the generalized gradient approximation of Perdew-Burke-Ernzerhof for  
98 the exchange-correlation term,<sup>30</sup> and find changes in thermal conductivity of less than 2%  
99 at room temperature.

100 Finally, we calculate the EPI for electron and hole concentrations varying from  $10^{17}$   
101 to  $10^{21}$   $\text{cm}^{-3}$ . The EPW code<sup>23</sup> is used to interpolate the EPI matrices as well as the  
102 electron and phonon eigenvalues from the coarse to the fine meshes. We chose a  $\mathbf{q}$ -mesh of  
103  $35 \times 35 \times 35$ , the same as in the phonon-phonon scattering calculations. We set the  $\mathbf{k}$ -mesh to  
104  $120 \times 120 \times 120$  and the Gaussian broadening to 2 meV. This gives less than 0.5% difference  
105 compared to results using  $144 \times 144 \times 144$  and 1 meV.

### 106 III. RESULTS AND DISCUSSION

#### 107 A. Phonon dispersion and electronic structure

108 The calculated phonon dispersion of 3C-SiC is shown in Fig. 1(a), in comparison with  
109 experimental data.<sup>31,32</sup> We find a gap of 3.5 THz between the highest acoustic phonon  
110 frequency and the lowest optical phonon frequency, in good agreement with the experimental  
111 results.<sup>31</sup> Such a gap inhibits three-phonon scattering processes involving optical and acoustic  
112 modes because of the energy and quasi-momentum conservation requirements, thus leading  
113 to longer phonon lifetimes. Fig. 1(b) shows the phonon density of states (DOS) and atom-  
114 resolved DOS. The three acoustic phonon branches at low frequencies are associated mostly  
115 with Si due to its heavier atomic mass, while the three optical branches at frequencies higher  
116 than 20 THz are associated with C.

117 The electronic band structure of 3C-SiC is shown in Fig. 1(c). The gap is indirect with  
118 the valence-band maximum at  $\Gamma$  and conduction-band minimum at X. The calculated band  
119 gap is 1.36 eV, compared to the experimental value of 2.36 eV.<sup>33</sup> This large error is due to  
120 the DFT-LDA deficiency in describing band gaps; by no means it will affect our conclusions  
121 regarding the effects of carriers on the thermal conductivity since the transitions across the  
122 gap do not contribute in our analysis. The electronic density of states is shown in Fig. 1(d).  
123 It shows that the density of states for holes is significantly larger than that for electrons,

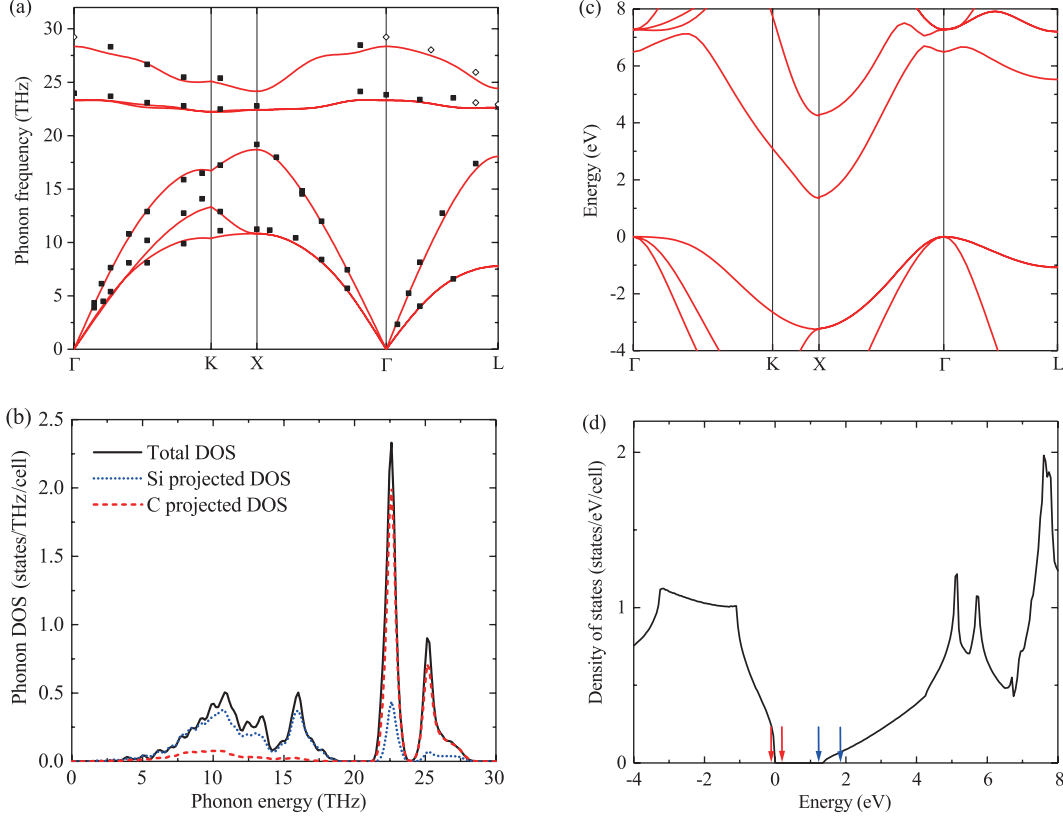


FIG. 1. (Color online) Phonon dispersion and electronic band structure of 3C-SiC. (a) Calculated phonon dispersion along with the experimental data (filled squares) from Ref. 31 and (open diamonds) from Ref. 32. (b) Total phonon density of states (black) and atom-resolved DOS: Si (blue) and C (red). (c) Calculated electronic band structure showing the indirect gap at  $\Gamma$ -X and (d) the total density of states near the valence- and conduction-band edges. We place the zero at the top of the valence band. The position of the Fermi levels for electron (blue) and hole (red) concentrations of  $10^{17}$  and  $10^{21}$   $\text{cm}^{-3}$  is indicated with arrows in (d).

124 and this will have important consequences for the effects of EPI on the thermal conductivity  
 125 as discussed later in the text.

## 126 B. Phonon scattering and lattice thermal conductivity in intrinsic SiC

127 The calculated lattice thermal conductivity ( $\kappa$ ) of bulk 3C-SiC, including the isotopic  
 128 effect, is shown in Fig. 2(a) along with experimental results.<sup>8,10,34</sup> At 300 K, we find  $\kappa$  is 491  
 129 W/mK, close to previous calculation of 479 W/mK.<sup>35</sup> We note that the theoretical results

130 are higher than the experimental values of Taylor<sup>34</sup> and Morelli.<sup>8</sup> This difference may be  
 131 related to the crystalline quality of the samples. For example, the results of Morelli *et al.*,  
 132 as the authors suggest, are affected by scattering from grain boundaries.<sup>8</sup> Therefore, it is  
 133 reasonable that our results for undoped bulk crystal end up higher than their experimental  
 134 values, especially at low temperatures where scattering by grain boundaries and other de-  
 135 fects dominate. At elevated temperatures, where phonon-phonon scattering dominates heat  
 136 transport in intrinsic semiconductors, the calculated results match well with the experimen-  
 137 tal values. We also find good agreement between our results for 3C-SiC and the experimental  
 138 values for 6H-SiC with N concentration of  $\sim 10^{17}$  cm<sup>-3</sup>,<sup>10</sup> where accurate in-plane results are  
 139 available. This is expected, since the local lattice configurations of 3C-SiC and 6H-SiC are  
 140 quite similar.

141 It is interesting to analyze how much each phonon branch contributes to the total thermal  
 142 conductivity at a given temperature. The calculated phonon-scattering rates for each of the  
 143 six phonon branches at 300 K is shown in Fig. 2(b). We find that the acoustic phonons,  
 144 especially low-frequency phonons, have the lowest scattering rates and therefore contribute  
 145 the most to the total thermal conductivity. At 300 K, the two transverse and one longitude  
 146 acoustic branches contribute with 38%, 32% and 28%, respectively. Indeed, we find that the  
 147 acoustic branches dominate at every studied temperature, contributing more than 95% of  
 148 the total thermal conductivity.

149 The phonon-resolved contribution to the total thermal conductivity can also give infor-  
 150 mation on the sample size effects on the heat transport. For instance, in nanostructures  
 151 or polycrystalline samples, heat transport may be limited by interface scattering. If the  
 152 characteristic diameter of the nanostructure or grain is less than the maximum mean free  
 153 path (MFP) of the phonons that contribute the most to the thermal conductivity, the ther-  
 154 mal conductivity will be lower than that of bulk at a given temperature. Fig. 3 shows the  
 155 cumulative thermal conductivity as a function of maximum MFP and phonon frequency at  
 156 room temperature.<sup>19</sup> The maximum MFP of a phonon mode  $\lambda$  is the product of its lifetime  
 157  $\tau_\lambda$  and the absolute value of the group velocity  $|\mathbf{v}_\lambda|$ . Using the method described in Ref. 19,  
 158 we find that MFP of the relevant heat carriers at room temperature is around 523 nm. We  
 159 also calculated the cumulative thermal conductivity as a function of phonon frequency, as  
 160 shown in Fig. 3. Our results show that phonons with frequencies below 12 THz contribute  
 161 with 95% of the total lattice thermal conductivity in intrinsic SiC.



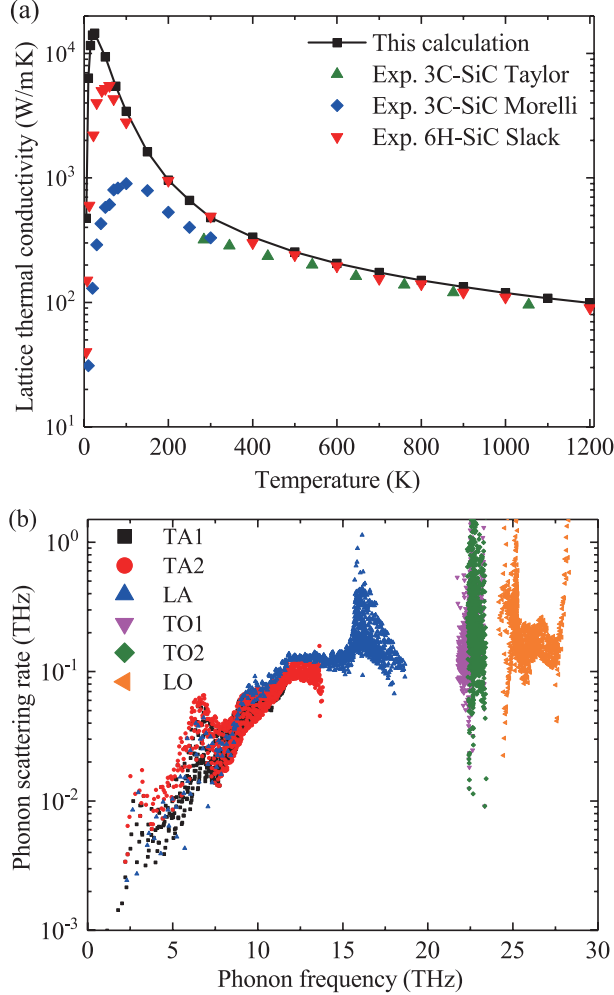


FIG. 2. (Color online) (a) Calculated lattice thermal conductivity (black square and solid line) of undoped 3C-SiC as a function of temperature. The experimental values for 3C-SiC are from Ref. 8 (diamonds) and from Ref. 34 (triangles). The experimental values for 6H-SiC (inverted triangles) in the planes perpendicular to the  $c$ -axis are from Ref. 10. (b) Phonon scattering rates for the six branches in intrinsic 3C-SiC at 300 K.

### 162 C. Effects of electron-phonon interaction on the thermal conductivity

163 Having discussed the lattice thermal conductivity in undoped SiC, we now present the  
 164 results for the effects of having electrons in the conduction band or holes in the valence  
 165 band on the thermal conductivity, i.e., how electron-phonon interaction affects the phonon-  
 166 scattering rates. We limit this study to the effects of the carriers only, neglecting their source  
 167 which can be either by introducing donor or acceptor impurities, or by light excitation where  
 168 both electron and holes are created. We note that we do not consider the phonon scattering

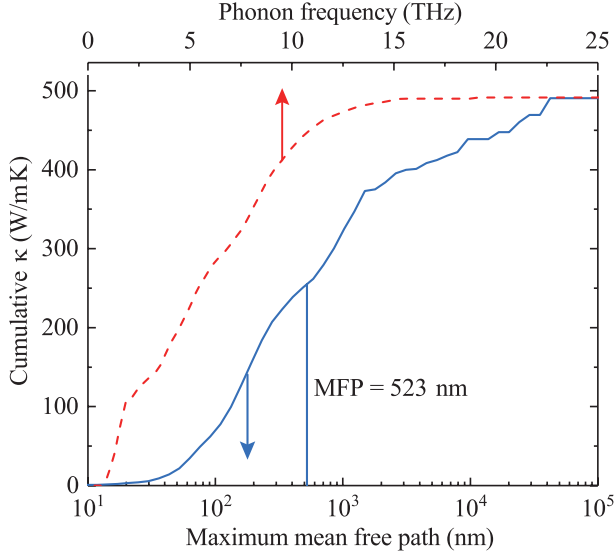


FIG. 3. Cumulative thermal conductivity of pure 3C-SiC as a function of the maximum mean free path and phonon frequency at 300 K.

169 by the impurities or defects that could be the source of the carriers. This effect may also  
 170 contribute to thermal conductivity in doped materials as recently discussed in Ref. 36.

171 First, we discuss the limit of very high carrier density. Figure 4 shows the phonon scatter-  
 172 ing rates that arise from electron-phonon interaction for carrier concentration of  $10^{21} \text{ cm}^{-3}$   
 173 in 3C-SiC at 300 K. For both electron-doped and hole-doped cases, the phonon scattering  
 174 rates from EPI are comparable to those from the three-phonon processes, especially for low-  
 175 frequency phonons (below 12 THz). Since the low frequency phonons contribute 95% of total  
 176 thermal conductivity in intrinsic 3C-SiC, our results show that electron-phonon scattering  
 177 significantly affects the thermal conductivity in 3C-SiC with high carrier concentrations.

178 We note that electron-phonon interaction in hole-doped 3C-SiC [Fig. 4(b)] is much  
 179 stronger than that in electron-doped material [Fig. 4(a)]. This difference can be inferred  
 180 from the energy and quasi-momentum conservation, and the electronic structure of 3C-SiC  
 181 near the band edges. Since the phonon energy is small, an electron or hole cannot transit to  
 182 conduction band from valence band; therefore, its initial and final electronic states remain  
 183 near the Fermi level, which resides near the valence-band edge in hole-doped or near the  
 184 conduction-band edge in electron-doped materials. In 3C-SiC, there are three bands near  
 185 the valence-band edge, with relatively small energy differences between them. Therefore,  
 186 holes can transit within a same band as well as jump between the three bands by absorbing

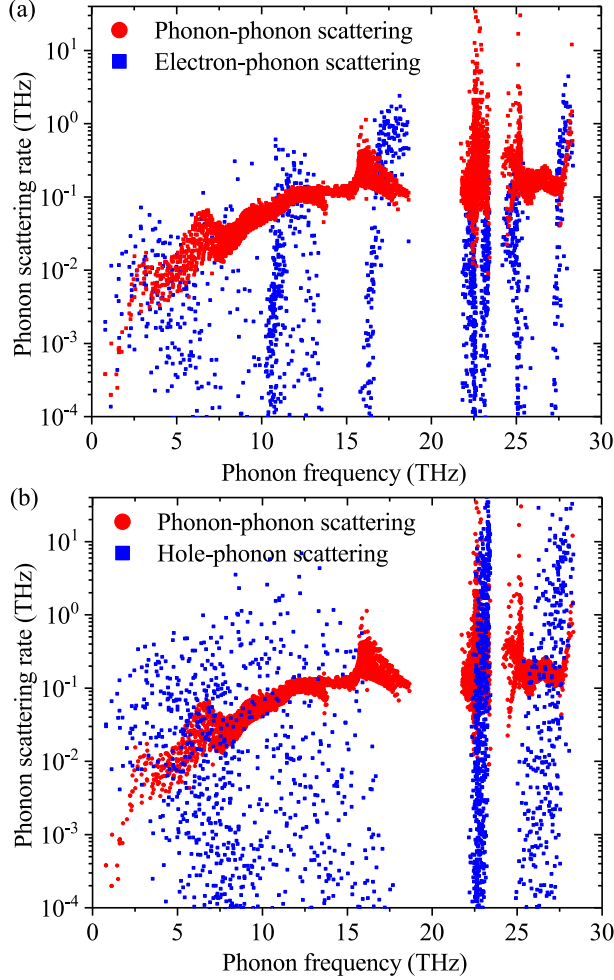


FIG. 4. (Color online) Phonon scattering rates from the intrinsic phonon-phonon scattering (red cycle) and electron-phonon interaction (blue square) at 300 K in 3C-SiC with (a) electron and (b) hole concentration of  $10^{21} \text{ cm}^{-3}$ .

187 or emitting phonons. In contrast, there is only a single band near the conduction-band edge,  
 188 and the electrons can only transit within this single band. In addition, as shown in Fig. 1(c)  
 189 the curvature of the bands near valence-band edge are lower than that of the conduction-band  
 190 edge, i.e., the effective masses of the holes are higher than that of the electrons,<sup>37</sup> translating  
 191 into higher density of hole states than electron states as shown Fig. 1(d). Therefore, be-  
 192 cause of the differences of electronic structure near valence-band and conduction-band edges,  
 193 electron-phonon scattering in hole-doped material is much stronger than in electron-doped  
 194 material. In other words, both the degeneracy of the hole bands and the heavier hole masses  
 195 lead to much higher scattering rates in hole-doped than in electron-doped 3C-SiC for the  
 196 same carrier density.

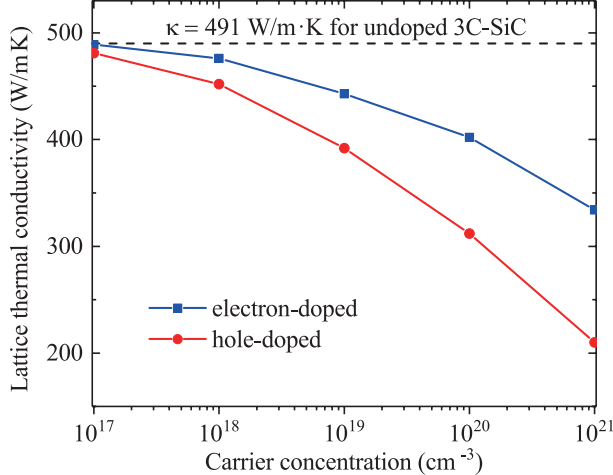


FIG. 5. (Color online) The lattice thermal conductivity  $\kappa$  as a function of carrier concentration in 3C-SiC, taking account of phonon-phonon scattering and electron-phonon interaction (EPI).

197 The calculated lattice thermal conductivity is shown in Fig. 5 for 3C-SiC with carrier  
 198 concentrations varying from  $10^{17} \text{ cm}^{-3}$  to  $10^{21} \text{ cm}^{-3}$  at 300 K. As discussed above, we find  
 199 that hole doping leads to lower thermal conductivities than electron 3C-SiC. Most notably,  
 200 we find a significant reduction in  $\kappa$ , from 491 W/m K for undoped material, to 392 and 210  
 201 W/m K, respectively, for hole concentrations of  $10^{19} \text{ cm}^{-3}$  and  $10^{21} \text{ cm}^{-3}$ . In contrast, for  
 202 the same electron concentrations we find that the thermal conductivity decreases to 443 and  
 203 334 W/m K. Recent yet unpublished work by Protik *et al.*<sup>38</sup> on 2H-SiC shows that the effect  
 204 of EPI leads to a decrease in the lattice thermal conductivity by 1% and 4.4% for electron  
 205 concentrations of  $10^{17} \text{ cm}^{-3}$  and  $10^{18} \text{ cm}^{-3}$ , respectively, in agreement with our calculation  
 206 for 3C-SiC.

207 The electron-phonon interaction also affects heat transport in nanostructured or poly-  
 208 crystalline samples, depending on their characteristic length. The cumulative thermal con-  
 209 ductivity of electron- and hole-doped 3C-SiC as a function of the MPF at 300 K are shown  
 210 in Fig. 6. With increasing electron or hole concentrations, the mean free path drops rapidly  
 211 due to the strong effect of electron-phonon interaction. The calculated mean free path drops  
 212 to 280 and 164 nm in electron- and hole-doped 3C-SiC, respectively, in the limit of very high  
 213 carrier concentration of  $10^{21} \text{ cm}^{-3}$ .

214 Finally, although all our calculations were performed for the 3C-SiC polytype, we expect  
 215 our results to be also valid for the 2H-, 4H-, and 6H-SiC polytypes. For instance, preliminary

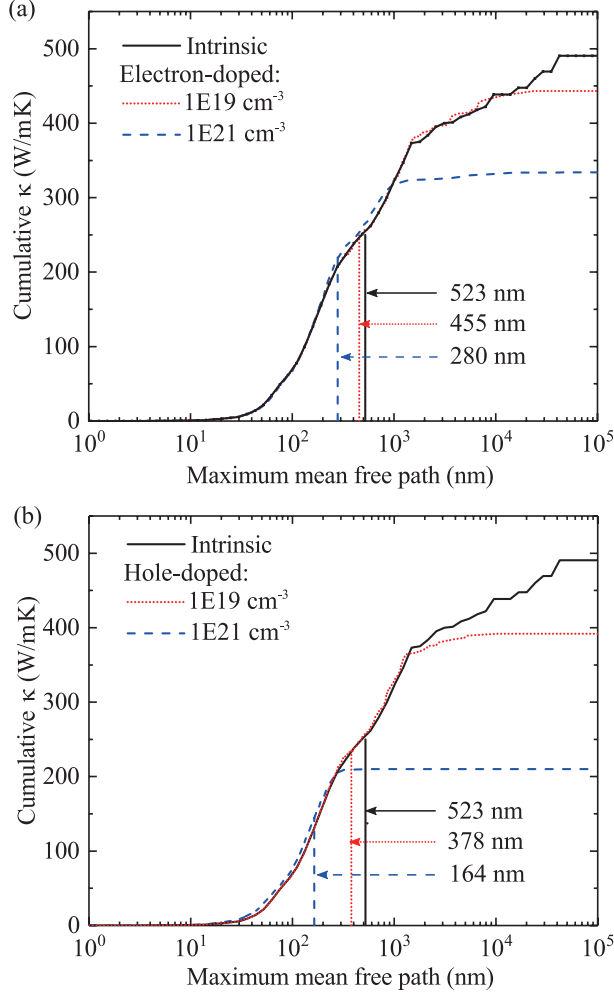


FIG. 6. (Color online) Cumulative thermal conductivity of electron- and hole-doped 3C-SiC as a function of the maximum mean free path at 300 K.

216 calculations for the lattice thermal conductivity in 2H-SiC show a very small anisotropy  
 217 in the phonon-scattering rates and thermal conductivity for undoped material. Since the  
 218 electronic density of states are quite similar we also expect that the effects of carriers on the  
 219 thermal transport to be similar in all these polytypes.

#### 220 IV. SUMMARY AND CONCLUSIONS

221 We calculated lattice thermal conductivity for intrinsic as well as electron- and hole-  
 222 doped 3C-SiC using first-principles methods. We predict a lattice thermal conductivity of  
 223 491 W/mK and a phonon mean free path  $\sim 523$  nm at 300 K for bulk 3C-SiC. We find that

224 electron-phonon interaction is much stronger in hole-doped than in electron-doped 3C-SiC,  
225 which is explained by the degeneracy of the valence-band edge and heavier hole masses. We  
226 predict that the room-temperature thermal conductivity significantly decreases from 491  
227 W/mK of intrinsic material to 210 and 334 W/mK in the limit of high hole and electron  
228 concentrations of  $10^{21}$  cm<sup>-3</sup>.

## 229 ACKNOWLEDGEMENTS

230 TW and CN gratefully acknowledge financial support from the II-VI Foundation, and  
231 AJ is grateful for the financial support from National Science Foundation under Grant No.  
232 1652994. This research was supported through the use of the Extreme Science and Engineer-  
233 ing Discovery Environment (XSEDE) supercomputer facility, National Science Foundation  
234 grant number ACI-1053575, and the Information Technologies (IT) resources at the Univer-  
235 sity of Delaware, specifically the high-performance computing resources.

---

236 <sup>1</sup> L. Patrick, D. R. Hamilton, and W. J. Choyke, Phys. Rev. **43**, 526 (1966).

237 <sup>2</sup> W. J. Choyke and G. Pensl, MRS Lulletin **22**, 25 (1997).

238 <sup>3</sup> P. Tanner, L. Wang, S. Dimitrijevic, J. Han, A. Lacopi, L. Hold, and G. Walker, Sci. Adv. Mater.  
239 **6**, 1 (2014).

240 <sup>4</sup> M. I. Lei and M. Mehregany, IEEE Trans. Electron Devices **60**, 513 (2013).

241 <sup>5</sup> Y. H. Zhu, J. C. Zhang, Z. T. Chen, and T. Egawa, J. Appl. Phys. **106**, 124506 (2009).

242 <sup>6</sup> M. Suemitsu, Y. Miyamoto, H. Handa, and A. Konno, e-Journal Surf. Sci. Nanotechnol. **7**, 311  
243 (2009).

244 <sup>7</sup> R. Yakimova, R. Vasiliauskas, J. Eriksson, and M. Syväjärvi, Mater. Sci. Forum **711**, 3 (2012).

245 <sup>8</sup> D. Morelli, J. Heremans, C. Beetz, W. Woo, G. Harris, and C. Taylor, in *Inst. Phys. Conf.*  
246 *Ser. No 137* (IOP Publishing Ltd, 1994) Chap. 3, pp. 313–316.

247 <sup>9</sup> J. R. Jenny, D. P. Malta, S. G. Müller, A. R. Powell, V. F. Tsvetkov, H. M. Hobgood, R. C.  
248 Glass, and C. H. Carter, J. Electron. Mater. **32**, 432 (2003).

249 <sup>10</sup> G. A. Slack, J. Appl. Phys. **35**, 3460 (1964).

- 250 <sup>11</sup> H. P. Phan, D. Viet Dao, P. Tanner, L. Wang, N. T. Nguyen, Y. Zhu, and S. Dimitrijevic, Appl.  
251 Phys. Lett. **104**, 111905 (2014).
- 252 <sup>12</sup> B. Liao, B. Qiu, J. Zhou, S. Huberman, K. Esfarjani, and G. Chen, Phys. Rev. Lett. **114**,  
253 115901 (2015).
- 254 <sup>13</sup> B. Liao, A. A. Maznev, K. A. Nelson, and G. Chen, Nat. Commun. **7**, 13174 (2016).
- 255 <sup>14</sup> N. Mingo, D. A. Stewart, D. A. Broido, L. Lindsay, and W. Li, in *Length-Scale Depend. Phonon*  
256 *Interact.*, edited by L. S. Shindé and P. G. Srivastava (Springer New York, New York, NY, 2014)  
257 pp. 137–173.
- 258 <sup>15</sup> P. Hohenberg and W. Kohn, Phys. Rev. **136**, B864 (1964).
- 259 <sup>16</sup> W. Kohn and L. J. Sham, Phys. Rev. **140**, A1133 (1965).
- 260 <sup>17</sup> S. Baroni, P. Giannozzi, and A. Testa, Phys. Rev. Lett. **58**, 1861 (1987).
- 261 <sup>18</sup> X. Gonze, Phys. Rev. A **52**, 1086 (1995).
- 262 <sup>19</sup> W. Li, J. Carrete, N. A. Katcho, and N. Mingo, Comput. Phys. Commun. **185**, 1747 (2014).
- 263 <sup>20</sup> M. Berglund and M. E. Wieser, Pure Appl. Chem. **83**, 397 (2011).
- 264 <sup>21</sup> J. M. Ziman, *Electrons and Phonons: The Theory of Transport Phenomena in Solids*, Interna-  
265 tional series of monographs on physics (OUP Oxford, 1960).
- 266 <sup>22</sup> F. Giustino, Rev. Mod. Phys. **89**, 015003 (2017).
- 267 <sup>23</sup> S. Poncé, E. Margine, C. Verdi, and F. Giustino, Comput. Phys. Commun. **209**, 116 (2016).
- 268 <sup>24</sup> N. Marzari, A. A. Mostofi, J. R. Yates, I. Souza, and D. Vanderbilt, Rev. Mod. Phys. **84**, 1419  
269 (2012).
- 270 <sup>25</sup> F. Giustino, M. Cohen, and S. Louie, Phys. Rev. B **76**, 165108 (2007).
- 271 <sup>26</sup> P. Giannozzi, S. Baroni, N. Bonini, M. Calandra, R. Car, C. Cavazzoni, D. Ceresoli, G. L.  
272 Chiarotti, M. Cococcioni, I. Dabo, A. Dal Corso, S. de Gironcoli, S. Fabris, G. Fratesi,  
273 R. Gebauer, U. Gerstmann, C. Gougoussis, A. Kokalj, M. Lazzeri, L. Martin-Samos, N. Marzari,  
274 F. Mauri, R. Mazzarello, S. Paolini, A. Pasquarello, L. Paulatto, C. Sbraccia, S. Scandolo,  
275 G. Sciauzero, A. P. Seitsonen, A. Smogunov, P. Umari, and R. M. Wentzcovitch, J. physics.  
276 Condens. matter **21**, 395502 (2009).
- 277 <sup>27</sup> J. P. Perdew and A. Zunger, Phys. Rev. B **23**, 5048 (1981).
- 278 <sup>28</sup> N. Troullier and J. L. Martins, Phys. Rev. B **43**, 8861 (1991).
- 279 <sup>29</sup> A. Taylor and R. M. Jones, *Proc. Conf. Silicon Carbide (Boston, MA 1959)*, edited by  
280 J. O'Connor and J. Smiltens (Pergamon Press, 1960) pp. 147–154.

- 281 <sup>30</sup> J. P. Perdew, K. Burke, and M. Ernzerhof, Phys. Rev. Lett. **77**, 3865 (1996).
- 282 <sup>31</sup> J. Serrano, J. Stremper, M. Cardona, M. Schwoerer-Bhning, H. Requardt, M. Lorenzen, B. Sto-  
283 jetz, P. Pavone, and W. J. Choyke, Appl. Phys. Lett. **80**, 4360 (2002).
- 284 <sup>32</sup> F. Widulle, T. Ruf, O. Buresch, a. Debernardi, and M. Cardona, Phys. Rev. Lett. **82**, 3089  
285 (1999).
- 286 <sup>33</sup> Y. Goldberg, M. Levinshtein, and S. Rumyantsev, *Prop. Adv. Semicond. Mater. GaN, AlN,*  
287 *InN, BN, SiC, SiGe*, edited by M. E. Levinshtein, S. L. Rumyantsev, and M. S. Shur (John  
288 Wiley & Sons, 2001) Chap. 5, p. 94.
- 289 <sup>34</sup> R. Taylor, H. Groot, and J. Ferrier, *TRPL 1336, Thermophys. Prop. Res. Lab. Rep.*, Tech.  
290 Rep. (Purdue University, 1993).
- 291 <sup>35</sup> L. Lindsay, D. a. Broido, and T. L. Reinecke, Phys. Rev. B **87**, 165201 (2013).
- 292 <sup>36</sup> A. Katre, J. Carrete, B. Dongre, G. K. H. Madsen, and N. Mingo, arXiv Prepr. (2017),  
293 arXiv:1703.04996.
- 294 <sup>37</sup> C. Persson and U. Lindefelt, Phys. Rev. B **54**, 10257 (1996).
- 295 <sup>38</sup> N. H. Protik, A. Katre, L. Lindsay, N. Mingo, and D. Broido, arXiv Prepr. (2017),  
296 arXiv:1705.02634v2.